Supporting Information

Graphene Sandwich Stable Perovskite Quantum-Dots Light Emissive Ultrasensitive and Ultrafast Broadband Vertical Phototransistors

*Krishna Prasad Bera[#‡], Golam Haider[†], Yu-Ting Huang[#], Pradip Kumar Roy[#], Christy Roshini Paul Inbaraj[//‡], Yu-Ming Liao[#‡], Hung-I Lin[#], Cheng-Hsin Lu[⊥], Chun Shen[⊥], Wan Y Shih[§], Wei-Heng Shih[⊥], and Yang-Fang Chen[#]**

[#]Department of Physics, National Taiwan University,
Taipei 106, Taiwan
*Email: yfchen@phys.ntu.edu.tw

[‡]Nano-Science and Technology Program, Taiwan International Graduate Program,
Academia Sinica
Taipei 106, Taiwan

[†]J. Heyrovský Institute of Physical Chemistry
Czech Academy of Sciences, Prague 8, Czech Republic

[//]Department of Engineering and System Science, National Tsing Hua University,
Hsinchu 300, Taiwan

[⊥]Department of Materials Science and Engineering
Drexel University, Philadelphia, PA 19104, USA

[§]School of Biomedical Engineering, Science, and Health Systems
Drexel University, Philadelphia, PA 19104, USA

Energy-Dispersive X-ray Spectroscopy (EDXS) Study

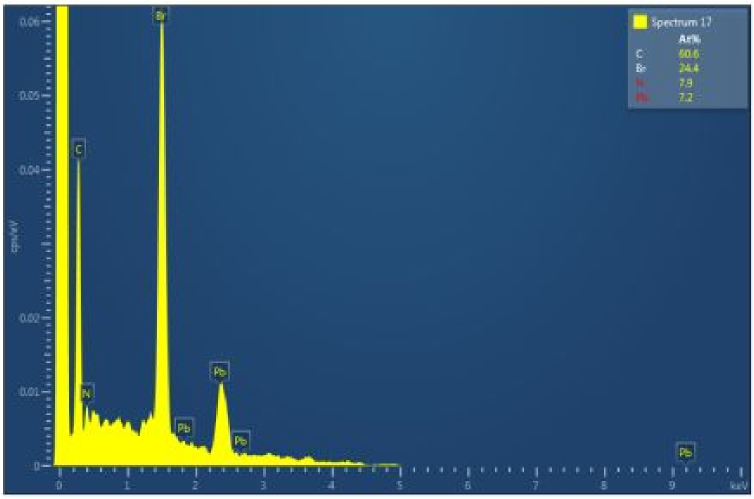

Figure S1. EDXS spectra of PQDs.

HRTEM Micrograph of PQDs over Large Area

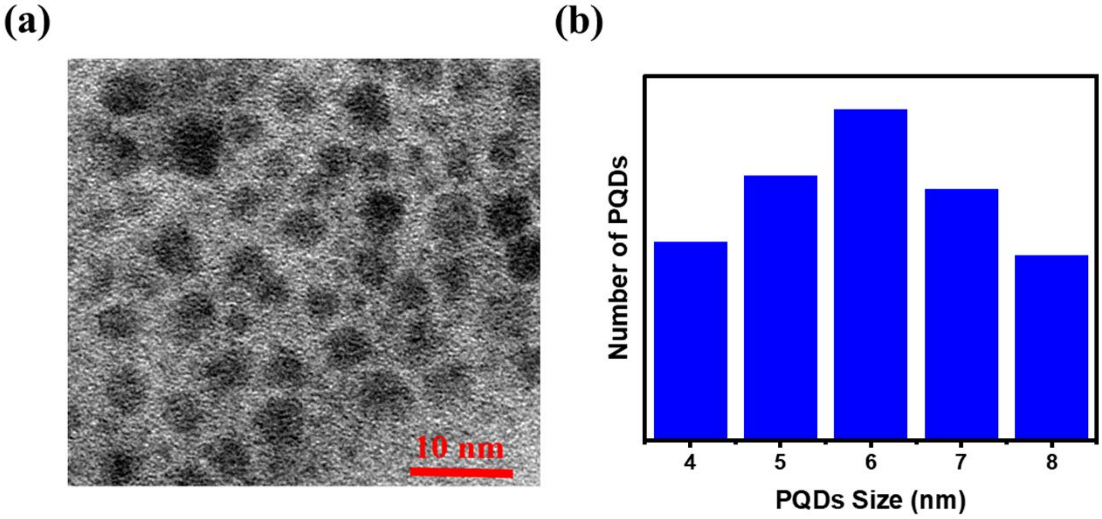

Figure S2. (a) HRTEM micrograph of the PQDs over large area. (b) The size distribution histogram of PQDs.

Raman Spectrum of Graphene

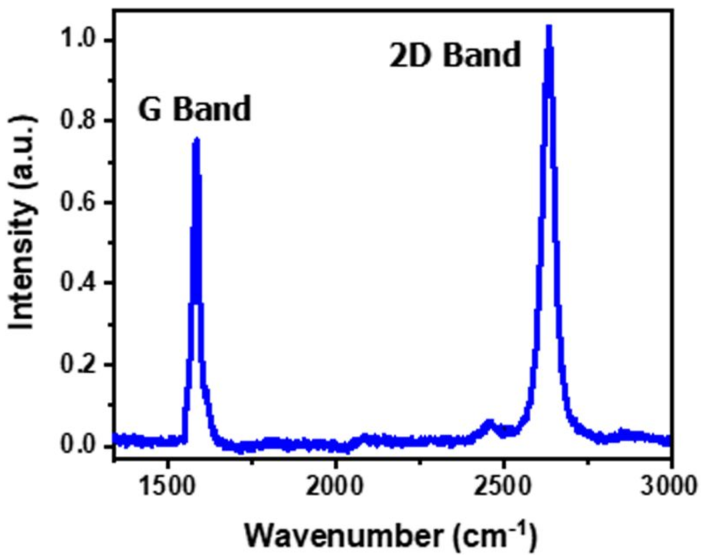

Figure S3. Raman spectrum of CVD graphene at 633 nm excitation.

The appearance of the Lorentzian shaped 2D band at 2640 cm^{-1} is sharper than the G band located at 1586 cm^{-1}, and the absence of a D band around ~ 1350 cm^{-1} indicates the presence of a high-quality graphene layer. The intensity ratio, I_G/I_{2D} of the 2D to the G peak was found to be < 1, and the 2D peak profile is Lorentzian in nature, which confirms that a single layer of graphene formed. Again, the absence of a D peak at ~ 1323 cm^{-1} indicates an almost defect-free high-quality graphene layer.[1,2]

Characterization of Mobility of Graphene

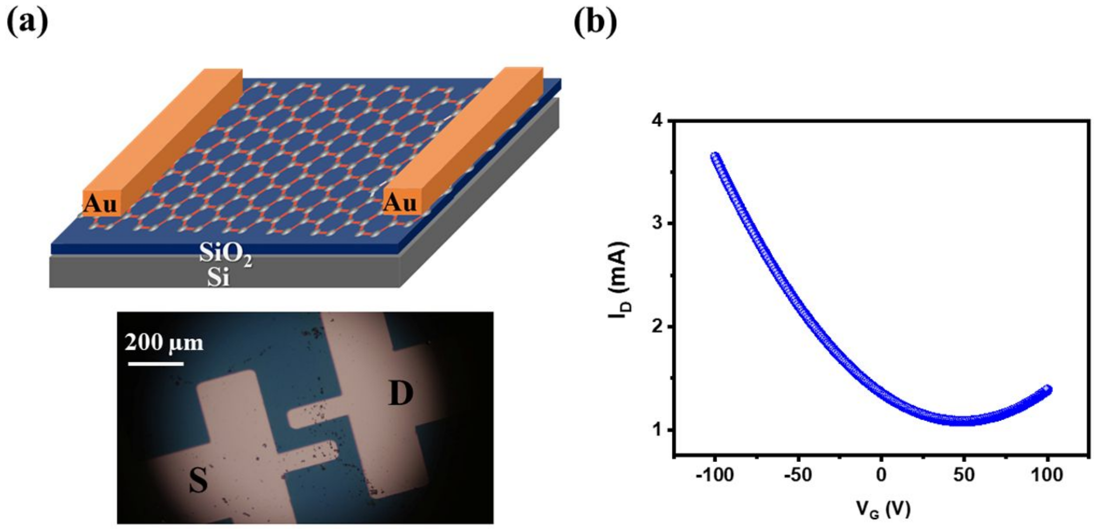

Figure S4. Estimation of the mobility of CVD graphene: (a) Schematic diagram with an optical microscope image of the transistor of monolayer graphene transferred on top of SiO_2/Si substrate for the measurement of carrier mobility. (b) Transfer characteristic, I_{DS} vs V_G, measured at a fixed drain to source voltage 1 V.

We have performed the gate dependent study of our synthesized monolayer CVD graphene by transferring it on SiO_2/Si substrate having a SiO_2 thickness 300 nm. The schematic of the device with an optical microscope image is shown in **Figure S3**. We estimated the mobility of the monolayer CVD graphene from transfer characteristic by using the following equation, $\mu_e = (L/WCV_{DS}) * (dI_{DS}/ dV_G)$, where $C = \varepsilon_0\varepsilon_r/d$ (with $\varepsilon_r = 3.9$, $\varepsilon_0 = 8.85 \times 10^{12}$ Fm^{-1}, and d = 300 nm being the relative permittivity and thickness of the insulating SiO_2 layer, respectively) is the capacitance per unit area estimated for gate dielectrics, L ≈ 100 μm is the channel length, and W ≈ 100 μm is the channel width.[3] The estimated value of dI_{DS}/dV_G from transfer curve is ~ 0.04 mAV^{-1}. Our estimated value of the graphene mobility is around 2.6×10^3 cm^2 $V^{-1}S^{-1}$.

The Transfer Characteristic of Graphene-PQDs Hybrid Device

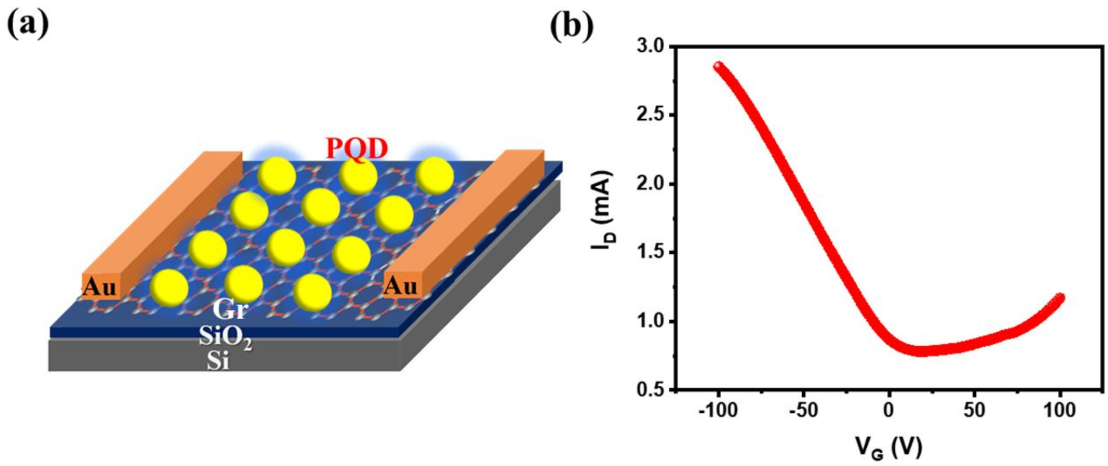

Figure S5. (a) Schematic of graphene-PQD hybrid device fabricated by spin coating of PQDs on top of the graphene. (b) The corresponding transfer characteristic.

CIE of Photoluminescence

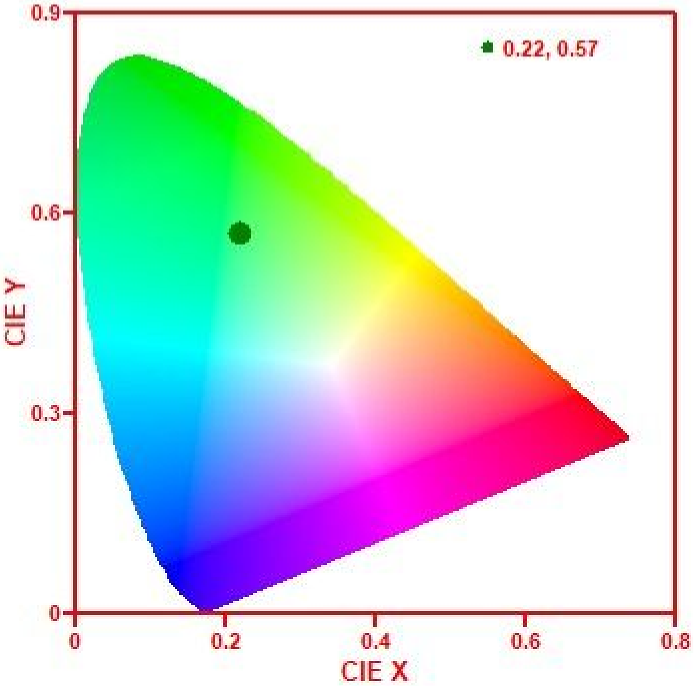

Figure S6. CIE chromaticity diagram corresponding to electroluminescence emission. The circle corresponds to the color coordinate (0.220, 0.570).

Absorption and Emission Spectra of Pure ligand

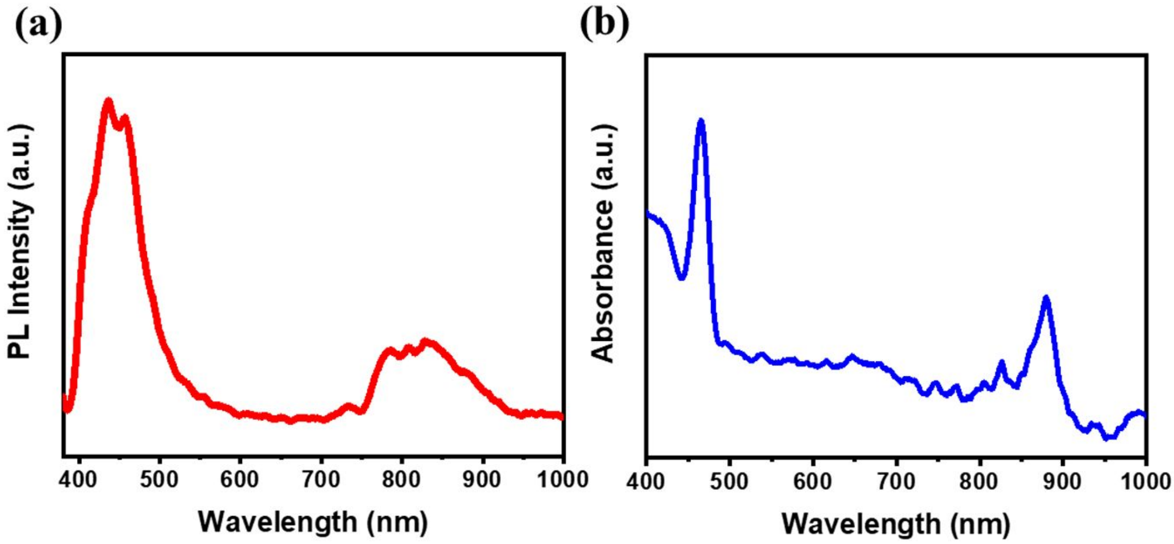

Figure S7. (a) Photoluminescence spectrum of pure capping ligand under the illumination by a 374 nm laser. (b) Absorption spectrum of pure capping ligand.

Raman Spectroscopy Study of PQDs

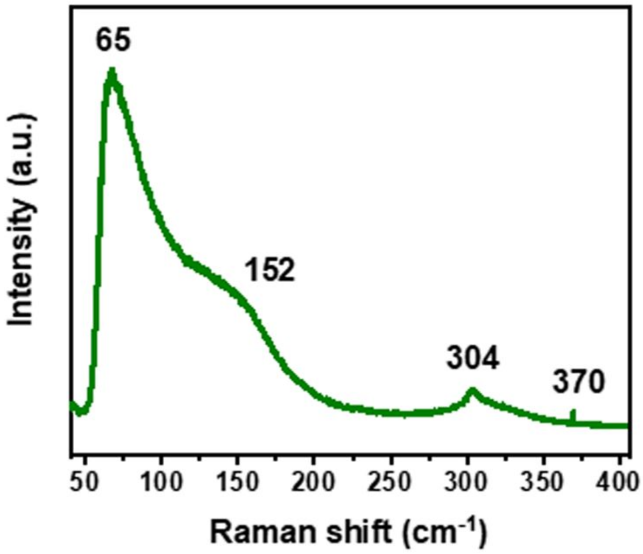

The band at 65 cm^{-1} indicates a clear marker of the presence inorganic component in the material. The bands at 64 and 110 cm^{-1} are assigned respectively to the bending and the stretching of the Pb-Br bonds. We also assign the librations of the organic cations at 156 cm^{-1}. The broad and unstructured 200 - 400 cm^{-1} feature is assigned to the torsional mode of the methylammonium cations. Raman peak at 303 cm^{-1} indicates the phonon mode corresponding to the rotation of the whole CH_3NH_3 cation around the C-N axis.[4,5]

Photograph of a Real Device with OM Image

(a)

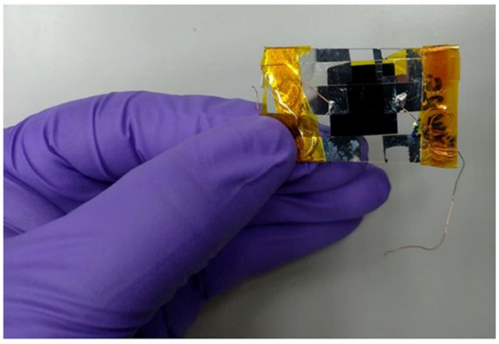

(b)

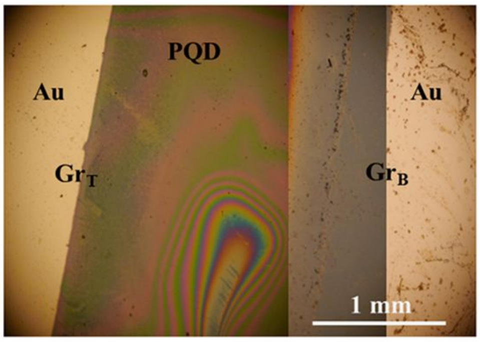

Figure S8. (a) Photograph of a real device by using commercial mobile camera. (b) Optical microscope image of the different portion of our fabricated device from the top view.

Device Optimization

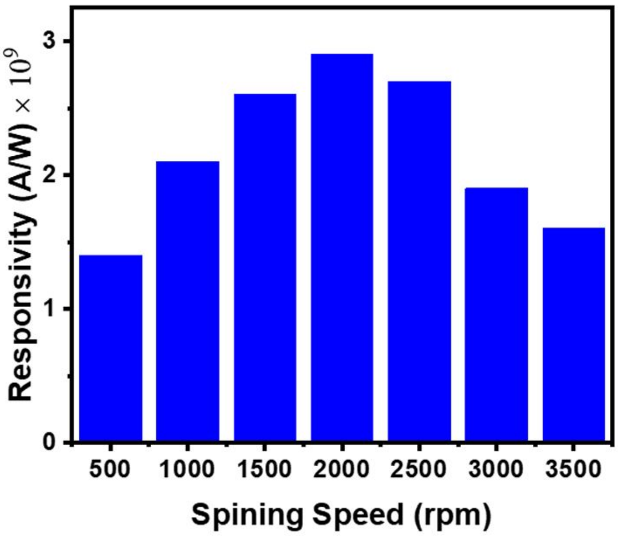

Figure S9. Device optimization by varying the thickness of PQDs through spin coating it on PDMS-graphene composite at the different spinning speed of the spin coater.

The Photoresponsivity

The photoresponsivity (R_{ph}), which is a measure of the electrical output per optical input of a photodetector and is described as the change in current in the photodetector device after the illumination of photons of various power levels, is defined as,[6]

$$R_{ph} = \frac{\Delta I(A)}{P(W)} \qquad , \qquad (1)$$

where ΔI in Ampere is the change in the channel current, *i.e.* $|\Delta I| = |\, I_{Illumination} - I_{Dark} \,|$, and P in Watt is the total illumination power on the device active area, *i.e.* 2 mm × 130 nm in this case. $|\Delta I|$ is around 11 µA at V_{SD} = 1 V for laser power density 1.2 nw/cm^2 with spot size ~ 0.03 cm^2 on the device area 130 nm × 2mm, as shown in **Figure 4b**. The reflectance spectrum of PQDs is shown in **Figure S7**. We estimated the value of the absorption coefficient of the PQDs ~ 4.46 × 10^6 m^{-1} at wavelength 457 nm. Our laser spot size (~ 0.03 cm^2) is larger than the device area (2 mm × 130 nm). All the calculations are normalized by the device active area.

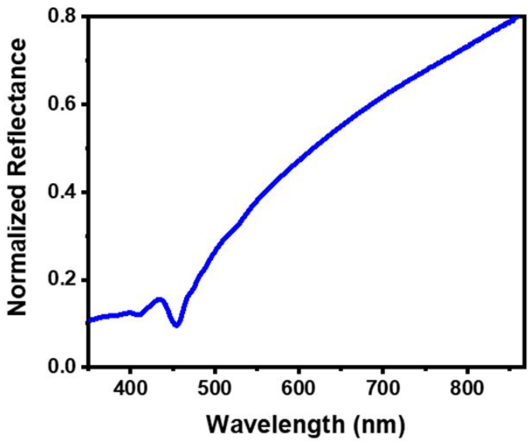

Figure S10. The reflectance spectra of PQDs.

The Specific Detectivity

Specific detectivity, which is one of the figures of merits of a photodetector used to characterize the performance of the photodetector, determines the minimum illumination light power that can be used to permit a detector to distinguish from noise, and it can be defined as,[7]

$$D^* = \frac{(AB)^{\frac{1}{2}}}{NEP} \quad , \qquad (2)$$

where A is the device active area, B is the measuring bandwidth which is inversely proportional to the response time of the photodetector and NEP is the noise equivalent power in units of Watt. NEP is the incident optical signal required to generate a photocurrent equal to the RMS noise current: NEP = $\frac{I_N}{R_{ph}}$, where I_N is noise current which is related with the dark current (I_D) of the photodetector and R_{ph} is the photoresponsivity of the device.[7] I_N^2 = 2eI_DB, where e is the electronic charge.[8]

External Quantum Efficiency

The external quantum efficiency of the vertical photodetector device has been calculated by using the following equation,[9]

$$EQE = \frac{|\Delta I|/q}{\Phi} \quad , \tag{3}$$

where q is the elementary charge, and $\Phi = P_{in}/E_{in}$ is the total incoming flux under the normal incidence illumination, P_{in} is the total power under normal incidence, and E_{in} is the energy per unit photon. Now, we know that photoresponsivity, $R_{ph} = \frac{|\Delta I(A)|}{P(W)}$, which is related with EQE by the formula, $R_{ph} = q \times \lambda \times EQE/hc$, where λ is the excitation wavelength.[10] By using the standard values of electronic charges, Plank constant, and light velocity we have calculated EQE = 3.89 × R_{ph} for the excitation wavelength λ = 457 nm. We estimated the value of the photoresponsivity ~ 3 × 10^9 AW^{-1} for same excitation wavelength as described in the supporting information of the photoresponsivity.

The Photocurrent Gain

The photocurrent gain (G) can be calculated using the following formula,[11]

$$G = \frac{\Delta I/q}{p/h\nu} \times \frac{1}{QE} \quad , \qquad (4)$$

where P is the incident laser power, $h\nu$ is the incident energy per photon, and QE is the quantum efficiency the of charge carrier generated per unit photon. In order to investigate the power variation of photocurrent gain, we further fitted the experimental values for photocurrent gain with the following formula,[11]

$$G = G^0 \times \frac{1}{1 + (\frac{P}{P_0})^n} \quad , \qquad (5)$$

where G^0 is a constant related to the drift carrier mobility and lifetime in the graphene/PQD/graphene composite, carrier transit time from the PQD to graphene $\tau_{transit}$, device dimension, *etc.* $G^0 = CT^0$, determines the highest photoresponsivity of the device, while the power P approaches zero, T^0 is the carrier lifetime at the lowest excitation energy. P_0 is the illumination power at which the surface states are fully occupied, and n is a phenomenological fitting parameter. The solid curve is the best fit with the parameters $P_0 = 1.41 \times 10^{-9}$ W and $n = 2.49$ as shown in **Figure 4d**. CT^0 is inversely proportional to $\tau_{transit}$. In order to achieve a higher gain, it is necessary to have a faster transit time and larger excited state carrier lifetime in the PQDs layer. The lower value of the illumination power while the surface trap states are saturated, $P_0 = 1.41 \times 10^{-9}$ W signifies that fewer defect states caused a decrease in the unwanted loss of photogenerated electrons, which is attributed to the high crystalline quality of PQDs. The higher value of n implies a better detection limit.

Electroluminescence Study

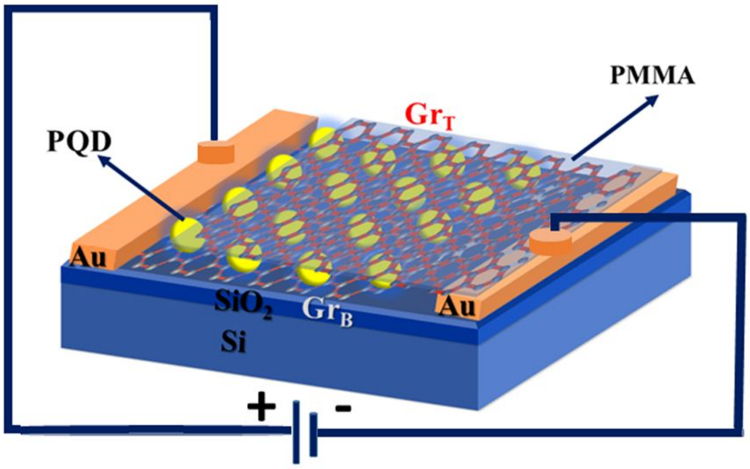

Figure S11. Schematic of the device with an applied electrical bias for electroluminescence study.

The Optical Photo of Light Emission

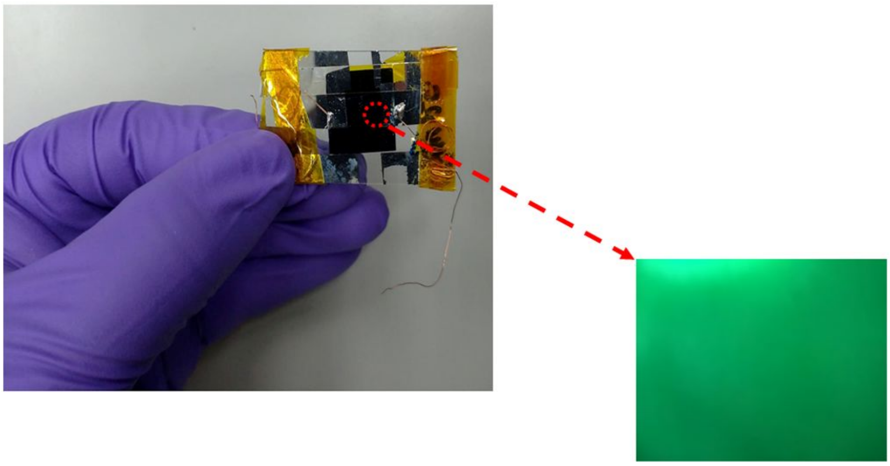

Figure S12. Optical photo of light emission from the phototransistor device with an indication of light emission location taken by using a commercial mobile camera.

External Quantum Efficiency Calculation of Light-emissive Phototransistor

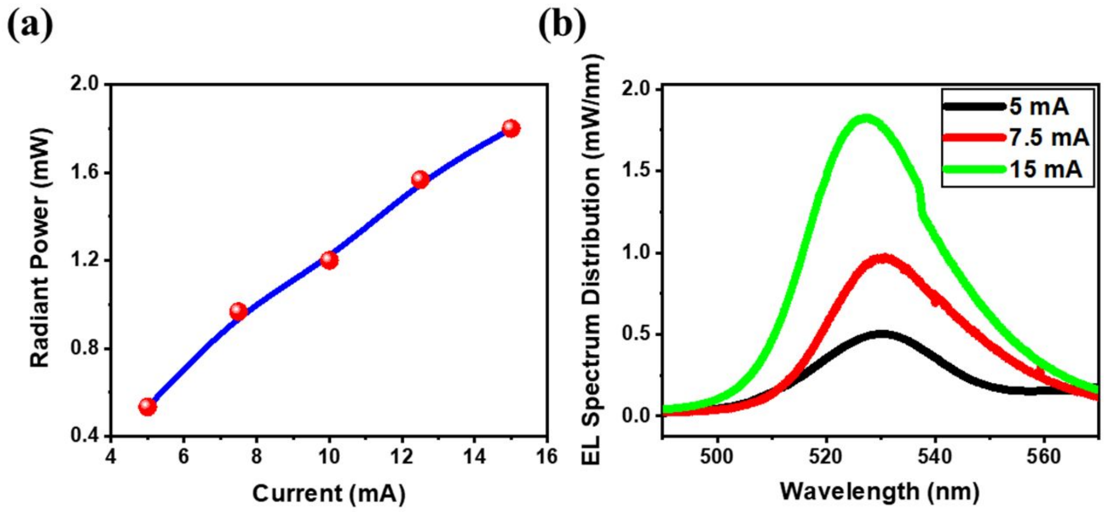

Figure S13. The estimation of EQE in light emission of phototransistor. (a)Variation of Radiant power as a function of forward current. (b) Emission spectrum distribution curve for different injection current in the device.

Typically, the overall efficiency of the LED device is characterized by the power efficiency (τ_{PE}), defined by the ratio of the radiant power (P) from the LED to the input electrical power, $\tau_{\mathrm{PE}} = \frac{radient\ power}{electrical\ power} = \frac{P}{IV}$, where I and V are the injection current and voltage in the LED device, respectively. The external quantum efficiency (EQE) of the LED device can be defined as the ratio of number of photons emitted from LED per second to the number of electrically injected electrons into LED per second, $\tau_{\mathrm{EQE}} = \frac{\#\ of\ photon\ emitted\ from\ LED}{\#\ of\ electrons\ injected\ into\ LED} = \frac{P/h\bar{v}}{I/q}$, where $h\bar{v}$ is mean photon energy and q is the electronic charge.[12] If LED device emits single-color light with a narrow-spectral width, the number of emitted photons will be P/hv (hv is the energy of a single photon).[12] If the spectral width cannot be neglected, then the mean photon energy can be defined as, $h\overline{\nu} \equiv \frac{P}{\int_0^\infty \frac{\lambda}{hC}\frac{dP(\lambda)}{d\lambda}d\lambda}$. The mean photon energy can be obtained from the electroluminescence spectrum distribution curve. In order to estimate the mean photon energy, we measured the EL spectrum distribution curve under different forward injection currents. For each injection current, we also measure the power of emitted light by power meter. The radiant power vs injection current plot is shown in **Figure S13a**. **Figure S13b** shows the EL spectrum distribution curve. We estimated the mean photon energy ($h\overline{\nu}$) ~ 2.3 eV from the emission spectrum distribution curves. We estimated EQE of our fabricated device ~ 5.6 % for the forward current injection 10 mA. We have tried to measure the emission with a large angle as wide as possible, and the obtained result is consistent with that estimated from the comparison with commercially available high brightness LED under the same experimental conditions, as shown in **Figure S14**.

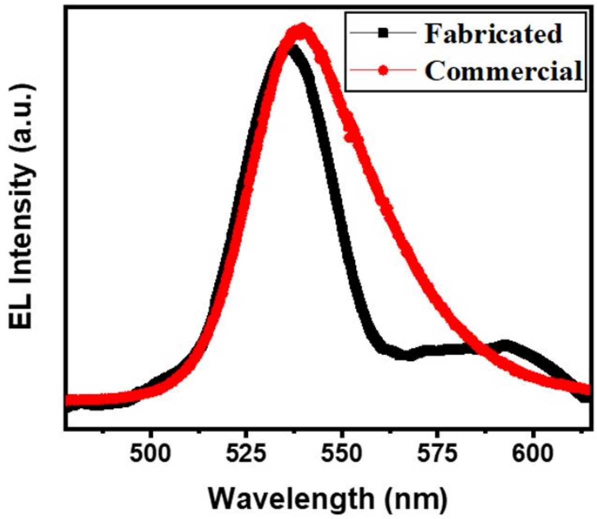

Figure S14. The comparison of the EL spectrum of our fabricated LED using PQDs with the EL spectrum of commercial green LED available in the market at similar input power.

REFERENCES

(1) Usman, M.; Haider, G.; Mendiratta, S.; Luo, T.-T.; Chen, Y.-F.; Lu, K.-L., Continuous Broadband Emission from a Metal-Organic Framework as a Human-Friendly White Light Source. *J. Mater. Chem. C* **2016**, *4*, 4728-4732.

(2) Ferrari, A. C.; Meyer, J. C.; Scardaci, V.; Casiraghi, C.; Lazzeri, M.; Mauri, F.; Piscanec, S.; Jiang, D.; Novoselov, K. S.; Roth, S.; Geim, A. K., Raman Spectrum of Graphene and Graphene Layers. *Phys. Rev. Lett.* **2006**, *97*, 187401.

(3) Tamalampudi, S. R.; Lu, Y.-Y.; Kumar U, R.; Sankar, R.; Liao, C.-D.; Moorthy B, K.; Cheng, C.-H.; Chou, F. C.; Chen, Y.-T., High Performance and Bendable Few-Layered Inse Photodetectors with Broad Spectral Response. *Nano Lett.* **2014**, *14*, 2800-2806.

(4) Quarti, C.; Grancini, G.; Mosconi, E.; Bruno, P.; Ball, J. M.; Lee, M. M.; Snaith, H. J.; Petrozza, A.; De Angelis, F., The Raman Spectrum of the $CH_3NH_3PbI_3$ Hybrid Perovskite: Interplay of Theory and Experiment. *J. Phys. Chem. Lett.* **2014**, *5*, 279-284.

(5) Wei, T.-C.; Wang, H.-P.; Li, T.-Y.; Lin, C.-H.; Hsieh, Y.-H.; Chu, Y.-H.; He, J.-H., Photostriction of $CH_3NH_3PbBr_3$ Perovskite Crystals. *Adv. Mater.* **2017**, *29*, 1701789.

(6) Long, M.; Gao, A.; Wang, P.; Xia, H.; Ott, C.; Pan, C.; Fu, Y.; Liu, E.; Chen, X.; Lu, W.; Nilges, T.; Xu, J.; Wang, X.; Hu, W.; Miao, F., Room Temperature High-Detectivity Mid-Infrared Photodetectors Based on Black Arsenic Phosphorus. *Sci. Adv.* **2017**, *3*, e1700589.

(7) Bera, K. P.; Haider, G.; Usman, M.; Roy, P. K.; Lin, H.-I.; Liao, Y.-M.; Inbaraj, C. R. P.; Liou, Y.-R.; Kataria, M.; Lu, K.-L.; Chen, Y.-F., Trapped Photons Induced Ultrahigh External Quantum Efficiency and Photoresponsivity in Hybrid Graphene/Metal-Organic Framework Broadband Wearable Photodetectors. *Adv. Funct. Mater.* **2018**, *28*, 1804802.

(8) Hou, C.; Yang, L.; Li, B.; Zhang, Q.; Li, Y.; Yue, Q.; Wang, Y.; Yang, Z.; Dong, L., Multilayer Black Phosphorus Near-Infrared Photodetectors. *Sensors* **2018**, *18*, 1668.

(9) Koppens, F. H. L.; Mueller, T.; Avouris, P.; Ferrari, A. C.; Vitiello, M. S.; Polini, M., Photodetectors Based on Graphene, Other Two-Dimensional Materials and Hybrid Systems. *Nat. Nanotechnol.* **2014**, *9*, 780.

(10) Shao, Y.; Liu, Y.; Chen, X.; Chen, C.; Sarpkaya, I.; Chen, Z.; Fang, Y.; Kong, J.; Watanabe, K.; Taniguchi, T.; Taylor, A.; Huang, J.; Xia, F., Stable Graphene-Two-Dimensional Multiphase Perovskite Heterostructure Phototransistors with High Gain. *Nano Lett.* **2017**, *17*, 7330-7338.

(11) Chiang, C.-W.; Haider, G.; Tan, W.-C.; Liou, Y.-R.; Lai, Y.-C.; Ravindranath, R.; Chang, H.-T.; Chen, Y.-F., Highly Stretchable and Sensitive Photodetectors Based on Hybrid Graphene and Graphene Quantum Dots. *ACS Appl. Mater. Interfaces* **2016**, *8*, 466-471.

(12) Shim, J.-I.; Shin, D.-S., Measuring the Internal Quantum Efficiency of Light-Emitting Diodes: Towards Accurate and Reliable Room-Temperature Characterization. *Nanophotonics* **2018**, *7*, 1601.